Calcif Tissue Int (1991) 48:407–413

Calcified Tissue International

Nucleation and Growth of Mineral Crystals in Bone Studied by Small-Angle X-Ray Scattering

Peter Fratzl,[1] Nadja Fratzl-Zelman,[2] Klaus Klaushofer,[2] Gero Vogl,[1] and Kristian Koller[2]

[1]Institut für Festkörperphysik der Universität Wien, Vienna, Austria; and [2]Ludwig Boltzmann Research Unit for Clinical and Experimental Osteology, 4th Medical Department, Hanusch Hospital, Vienna, Austria

Summary. The mechanism of calcification in bone and related tissues is a matter of current interest. The mean size and the arrangement of the mineral crystals are important parameters difficult to obtain by electron microscopy. Furthermore, most studies have been carried out on poorly calcified model systems or chemically treated samples. In the work presented here, native bone was studied as a function of age by a quantitative small-angle X-ray scattering method (SAXS). Bone samples (calvariae and ulnae) from rats and mice were investigated. Measurements were performed on native bone immediately after dissection for samples up to 1 mm thick. The size, shape, and predominant orientation of the mineral crystals in bone were obtained for embryonal, young, and adult animals. The results indicate that the mineral nucleates as thin layers of calcium phosphate within the hole zone of the collagen fibrils. The mineral nuclei subsequently grow in thickness to about 3 nm, which corresponds to maximum space available in these holes.

Key words: Bone — Mineral crystals — Small-angle X-ray scattering — Hydroxyapatite — Biomineralization.

Various theories now agree that mineralization occurs by a heterogeneous nucleation of hydroxyapatite (HA) out of a solution containing calcium and phosphate ions. However, at the present time, the mechanisms of mineral deposition within the organic matrix of bone are still poorly understood. Nucleation of HA due to the removal of biological inhibitors, to interaction with calcium-binding protein molecules, or to precipitation out of a locally supersaturated calcium phosphate solution are currently discussed as possible mechanisms [1, 2]. In this context the knowledge of size and shape of bone crystals is of primary importance.

Among the techniques providing sufficient resolution to investigate single mineral crystals, electron microscopy is the most widely used one [2–5]. The determination of the average crystal size by electron microscopy, however, is difficult because for each individual crystal, serial tilts of the sample have to be performed in order to avoid artifacts due to spatial overprojection [4].

Fully mineralized bone can also be investigated by X-ray [2, 5, 6, 7] or neutron scattering [8] techniques. Compared to electron microscopy, the use of X-ray diffraction, including analysis of the linewidth, has the advantage of directly providing an average crystal size. However, the results obtained by this method are ambiguous because not only the crystal size but also strain and imperfection of the crystallinity contribute to the broadening of the X-ray lines [7].

We present a detailed study of the calcification process in native bone using quantitative small-angle X-ray scattering (SAXS). In contrast to X-ray diffraction, where the broadening of lines from the internal structure of the crystals is interpreted, SAXS analysis uses the broadening of the primary beam which is insensitive to strain as well as to crystal imperfections and depends exclusively on the outer dimensions of the crystals. In fact, SAXS is a powerful method for investigating size, orientation, and arrangement of particles ranging between 0.5 and 50 nm [9]. As the scattering is pro-

Send reprint requests to P. Fratzl, Institut für Festkörperphysik der Universität Wien, Strudlhofgasse 4, A-1090 Vienna, Austria

portional to the square of the electron density, the contribution from all organic components of bone is small compared to the scattering from HA. SAXS therefore provides selective information about size and arrangement of HA crystals without perturbation from other components [10]. SAXS with a conventional Kratky camera has previously been used [11], in comparison with gas absorption data, to determine the specific surface of the bone mineral. In contrast, in this study we used an experimental setup with circular pinholes, which avoids many difficulties due to the line focus of the Kratky camera [9] and provides reliable information on the mean size and orientation of the mineral crystals.

Materials and Methods

Bone samples were taken from mice (strain Him:OF1/SPF) and rats (strain Him:OFA/SPF, Institute for Experimental Animal Research of the University of Vienna, Himberg) between the 18th day of gestation and the 300th day after birth. They were investigated by SAXS either immediately after dissection or after storage up to 3 days in cold acetone, which did not alter the diffraction patterns. Without further preparation steps, the samples were transferred into the measuring device where they were held in high vacuum. Calvariae were mounted with their great surface and ulnae with their cylinder axis perpendicularly to the X-ray beam. The use of a rotatable, linear, position-sensitive detector permitted the recording of the radiation scattered parallelly to the bone axis (axial scattering) and the scattering normal to this axis (radial scattering) without moving the sample.

The experimental setup consisted of a 12 kW rotating anode X-ray generator used in a point-focus geometry and the X-ray beam had a circular cross section of 0.5 mm^2. The radiation wavelength was 1.54 Å or 0.71 Å corresponding to Cu-Kα and Mo-Kα radiation in combination with Ni and Zr filters, respectively. Before each measurement, the transmission coefficient of the sample was determined by measuring the reduction of the scattering from glassy carbon after introducing the sample as absorber into the primary beam. The SAXS spectra were then recorded for several hours up to 1 day, depending on the counting statistics. Data correction was performed by subtracting the background measured without sample from the spectra divided by the experimentally determined transmission coefficient.

Results

Long Bones

Typical results of the SAXS measurements are shown in Fig. 1. The scattering intensity I(q) was plotted on double logarithmic scales versus $q = (4\pi/\lambda)\sin(\theta/2)$; θ is the scattering angle and λ the wavelength of the incident X-ray beam. In Fig. 1 the radial and the axial components of the scattering from the midshaft region of an ulna (300 days old, adult mouse) are shown. First, notice that the axial part of the scattering was much lower than the radial part, indicating that the crystals were elongated and oriented parallelly to the bone axis. Secondly, the axial component showed a series of maxima which were located at positions defined by $q = 2\pi n/D$ ($n = 1,2,3,4,5, \ldots$), which is the fingerprint of a periodic arrangement of the crystals in axial direction with a period D (Fig. 1). The distance D was determined to be 67 nm which corresponds exactly to the axial macroperiod of the holes between the collagen molecules according to the Hodge-Petruska scheme [12].

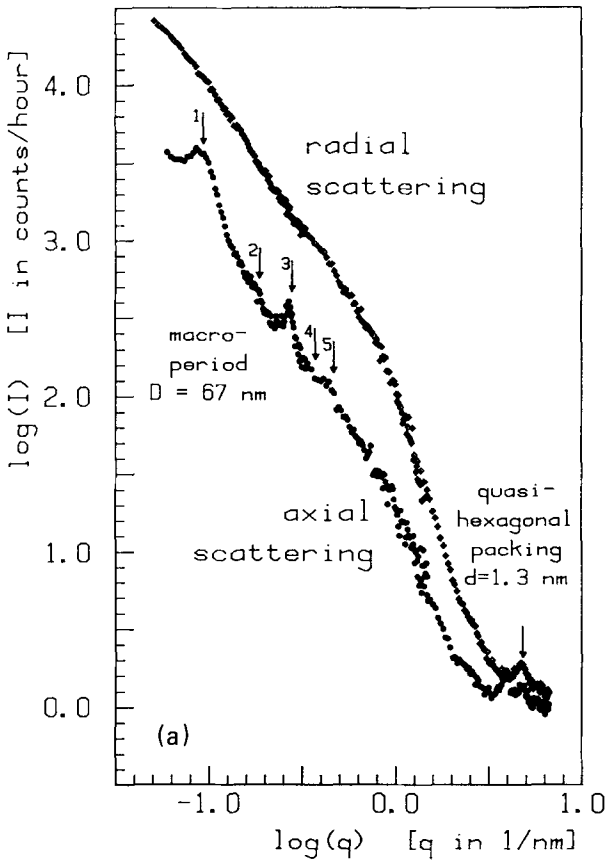

Fig. 1. Radial and axial scattering from the ulna (midshaft region) of an adult mouse. (I) is the scattered intensity and (q) depends on the scattering angle as defined in the text. Log means the decimal logarithm. The numbered arrows indicate the positions of the first five orders of the reflections expected from fibril holes filled with HA and arranged according to the Hodge-Petruska scheme with an axial period of (D) = 67 nm. (d) is the distance between adjacent collagen layers in the quasi-hexagonal packing model.

In the radial scattering, a broad peak appeared for q equivalent to d = 1.3 nm, the same distance as between adjacent planes in the quasi-hexagonal packing of the collagen molecules [13]. There was, however, no other peak in the radial scattering from the fully mineralized bone for distances larger than 1.3 nm (Fig. 1). In particular, the peak at 3.8 nm reported for the scattering from unmineralized col-

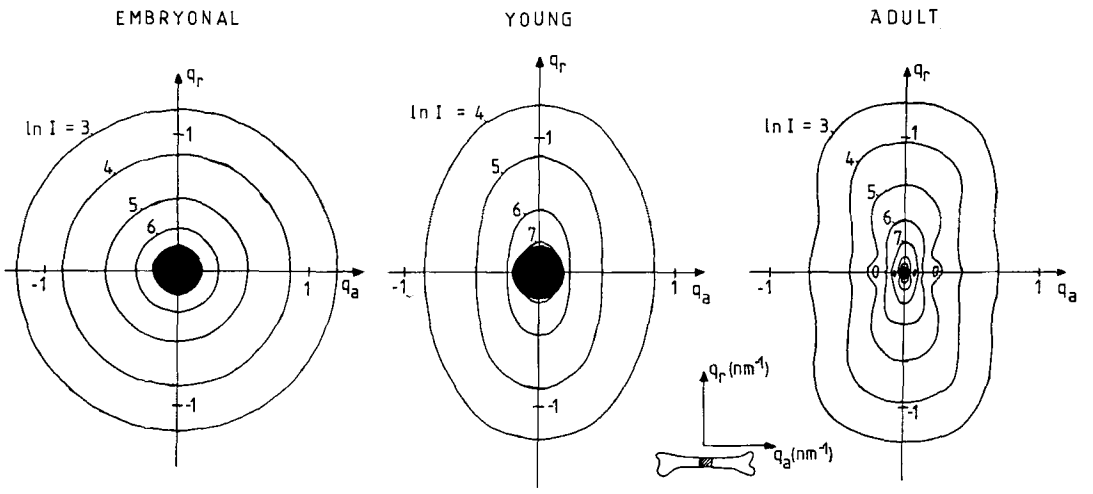

Fig. 2. Isointensity contours of the scattering from the ulna (midshaft region) of an embryonal (19 days after conception), a young (5 days old), and an adult (100 days old) mouse. The numbers close to the contours indicate the natural logarithm of the intensity expressed in counts per minute. (q_a) and (q_r) correspond to q (definition see text) in axial and radial direction of the bone, respectively. The black circle indicates the size of the lead foil used to stop the primary beam. Sections through the scattering from adult ulnae along q_a (axial scattering) and q_r (radial scattering) correspond to the curves shown in Fig. 1.

lagen from rat tail tendons [13, 14] was not found in our samples. As the existence of a typical distance between the crystals should induce a maximum in the SAXS pattern [9, 15], our data exclude the formation of arrays of crystals arranged periodically in radial direction with a period larger than 1.3 nm.

The age dependence of the anisotropy of the SAXS from the midshaft region of ulnae is shown in Fig. 2. The scattered intensity is represented as equiintensity contours for embryonic, young, and adult bones. The more and more pronounced anisotropy of the isointensity contours from the embryonal to the adult state may be interpreted as the progressive alignment of elongated crystals along the principal axis of the bone. Suppose that the crystals are much smaller in radial than in axial direction: The trace in the plane shown in Fig. 2 from a single isolated crystal would then correspond to a thin streak. Considering the "fan-like" intensity in the adult mouse (Fig. 2c) as formed by the superposition of streaks from differently oriented crystals, one can roughly estimate that the orientation of the HA needles was mostly distributed in the range of 0 to 30° measured between the long dimension of the crystal and the main axis of the bone. This corresponds well to the dominant orientation of the osteons in this type of bone and is in good agreement with more quantitative evaluations of crystal orientation in mature bone by SAXS [16] as well as other methods [17].

Calvariae

In contrast to ulnae where the scattering was different in radial and in axial direction (Fig. 1), a completely isotropic SAXS was obtained from all calvariae. Figure 3 shows typical scattering curves for calvariae at different ages. The overall intensity of the scattering curves increased with age due to higher mineral content in the samples. As shown in Fig. 3, all curves were behaving for high q values as Pq^{-4} according to Porod's law [9]. The Porod constant P is known to be proportional to the specific surface of the mineral in the sample [9, 11, 15]. Moreover, all scattering curves could be fitted using the form factor of needles [15] $F(q) = 4\pi^2[J_1(qR)]^2/q^3$ (J_1 is the Bessel function of the first kind) averaged with a continuous distribution of the needle radius R around a mean value R_0. Independent of the choice of the distribution function (gaussian, Poisson, etc.), the fit remained unchanged as long as the standard deviation of the distribution was $\approx R_0/2$. We finally show fits by full lines in Fig. 3, obtained by averaging the form factor with the continuous distribution $x^3e^{-x}dx/6$ (with $x = 3R/R_0$). For comparison, the shape factor for plates averaged in the same manner was also figured. Note that the scattering functions for needles behave as q^{-1} at small q whereas for plates the behavior is q^{-2} [15]. Again, there was no maximum or irregularity in the diffraction curve which would indicate any type of periodic ordering of the crystals within the "quasi-hexagonal" lattice in the equatorial plane.

Determination of Crystal Thickness

One possibility to determine the average thickness

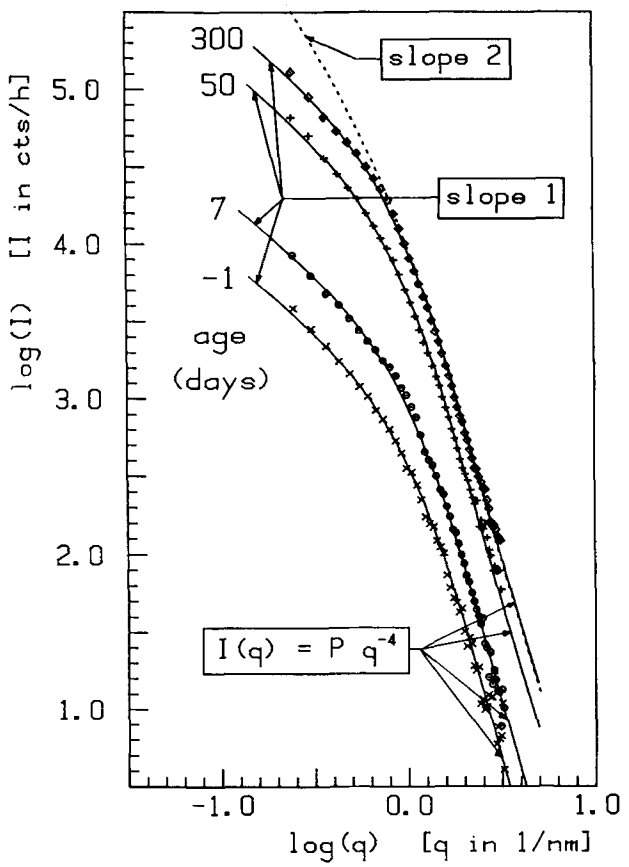

Fig. 3. Scattering from the calvariae of mice at different ages as indicated in the Fig. (age −1 means embryonal at the 20th day of gestation). In contrast to ulnae where differences existed between radial and axial scattering (Fig. 1), the scattering from each calvaria was isotropic and is therefore represented by one curve only. The full lines are calculated curves fitted to the data points by using the shape function of long cylinders averaged with a distribution of the thickness around its mean value (see text). The broken line shows the calculated curve with the shape function of plates averaged in the same way, which cannot describe our data. All data follow the Porod law: $I(q) = Pq^{-4}$ for high q values.

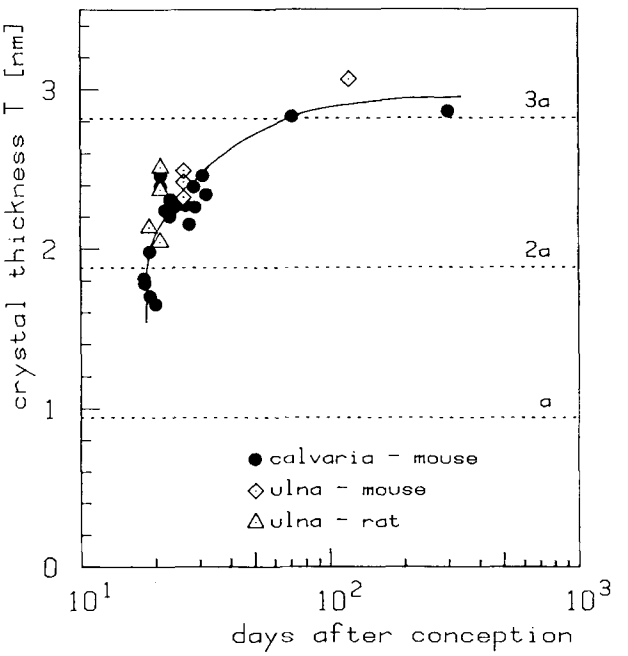

Fig. 4. Average thickness of the HA crystals as function of time (in days after conception). Mice and rats were born on the 23rd and 21st day after conception, respectively. The broken lines show the theoretical thickness of crystals made by exactly one, two, or three layers of HA (a = 0.94 nm is the lattice parameter of HA). The full line is a guide to the eye.

of the crystals would be fitting a model function to the data as shown in Fig. 3. In the present study we used a more general approach, which did not need any assumption on the shape of the mineral particles. First, we found that in all cases the scattering intensity I(q) followed the Porod law [9, 11, 15], i.e., a behavior like Pq^{-4}, in the limit of high q values (Figs. 1 and 3). A general expression for the Porod constant P is given by $P = [S/(\pi V)]\int_0^\infty q^2 I(q)dq$, where V is the total volume of the crystals, S their total surface and I(q) the spherically averaged scattering intensity [15]. Both the integral intensity $\int_0^\infty q^2 I(q)dq$ and the Porod constant P were determined from each scattering function I(q). Thus, without any model for the shape of the crystals, it was possible to compute the ratio of surface to volume of the crystals. Consequently, we obtained the parameter T = 4V/S, which characterizes their smallest dimension. In particular, for needle-shaped crystals, T represents exactly the average diameter of the needles. T was determined for all samples in the way described above and plotted versus age (Fig. 4). The age dependence of the crystal thickness T was characterized by a rapid increase at the beginning of the calcification process followed by a saturation (Fig. 4); this saturation is in agreement with previous observations [1].

Discussion

The SAXS of long bones and calvariae from mice and rats showed that the bone crystals were elongated even at the earliest stages of mineralization (at the 18th day of gestation). The axial scattering from long bones (Fig. 1) exhibited maxima analogous to those observed for collagen which have been explained by the Hodge-Petruska scheme [12]: The collagen molecules are arranged parallely and they are shifted axially by multiples of D = 67 nm. The length of molecules are 4.4 D; this staggering induces gap regions of width 0.6 D altenating with

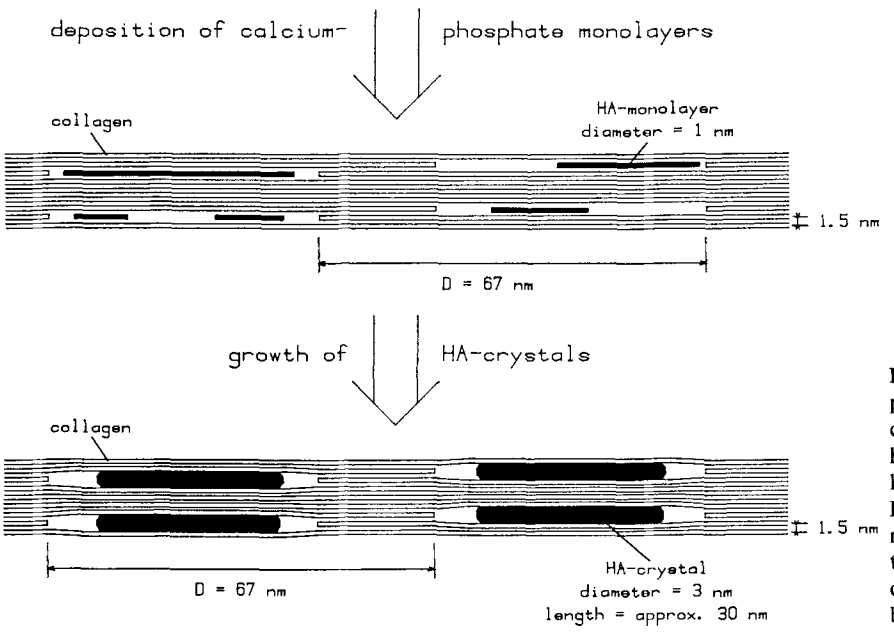

Fig. 5. Model for the calcification process: At first, monolayers of calcium phosphate are formed within the hole zones of the fibrils. Then these layers increase in thickness forming HA crystals until they reach the maximum thickness of 3 nm. Notice that crystals of this size already slightly compress the collagen microfibrils in between them.

overlap region of width 0.4 D. Consequently, one fifth of the sites occupied by collagen molecules in the overlap regions are unoccupied in the gap regions, therefore creating holes.

In principle, the maxima observed in the scattering from fully mineralized bone (Fig. 1) could arise from unmineralized collagen fibrils coexisting with mineralized regions. Nevertheless, as the peaks in Fig. 1 are quite prominent (remember the logarithmic scales), we believe they were due to mineral located within holes rather than to unmineralized fibrils. In fact, their scattering intensity is proportional to the square of the difference in electron density between gap and overlap regions. For water-filled holes, we estimate (a numerical value for the density of collagen was taken from [18]) the contrast to be in the order of $(\Delta Z_1)^2 = [1/5\ (Z_{collagen} - Z_{water})]^2 = [1/5\ (0.74\text{–}0.56)\ mol/cm^3]^2 = 1.3\ 10^{-3} (mol/cm^3)^2$ where Z is defined as the number of electrons per volume counted as multiples of mol/cm^3, i.e., 6.10^{23} electrons per cm^3. Similarly, the contrast for HA-filled holes with the collagen fibrils would be $(\Delta Z_2)^2 = [1/5\ (Z_{collagen} - Z_{HA})]^2 = [1/5\ (0.74\text{–}1.57)\ mol/cm^3]^2 = 27.6\ 10^{-3}\ (mol/cm^3)^2$ which is higher by a factor of about 21. If we now take into account that in fully mineralized bone (which corresponds to the curve shown in Fig. 1) the mineral represents 75% in weight [18], which means more than half of the total bone volume, it is not very likely that a significant contribution to the scattering arises from unmineralized collagen fibrils. Therefore, we conclude that the maxima in the axial scattering in Fig. 1 are mainly due to mineral arranged spatially in the same manner as the holes in the collagen fibrils and therefore most likely within them. A rough estimation of the crystal length in axial direction could be made by noting that the odd orders of the maxima in the axial scattering (n = 1,3,5) were particularly well pronounced whereas the even orders were much smaller (Fig. 1). The same features were found in calcified tendon [19] where the typical crystal length was estimated to be half the period D = 67 nm, i.e., approximately 30 nm.

The average thickness T of the crystals was determined as function of the age of the animal (Fig. 4). It appeared that the thickness of the elongated crystals in embryonal bone was about the size of one unit cell of hydroxyapatite. Indeed, HA is hexagonal with c = 0.69 nm and a = 0.94 nm [20], the c-axis being parallel to the collagen fibrils [7]. It seems, therefore, most likely that the crystals nucleate as thin layers within the hole zones of the collagen, where collagen itself or collagen-associated calcium-binding molecules, e.g., phosphoproteins [2], probably act as substrates. The thickness of HA crystals increased with age to about 3 nm, which corresponds to the maximum space available within the holes, indicating a simple steric inhibition of further crystal growth. These results are summarized in Fig. 5. Three questions arise from the order of magnitude of T. First, in embryonic bone the crystals are already very long but have a lateral extension of only one or two lattice parameters. Therefore the (002) line should be well observable in the wide-angle X-ray diffraction

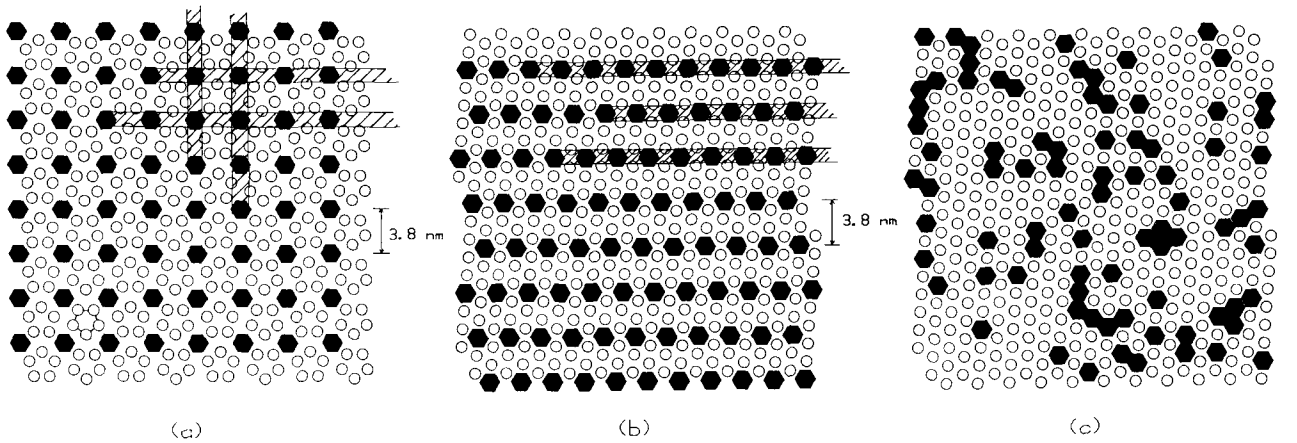

Fig. 6. Three possible equatorial arrangements of HA crystals within the collagen fibrils (circles) according to **(a)** Microfibrilar model: The HA-crystals (hexagones) are located in tunnels between microfibrils formed by five adjacent collagen molecules [22]. One such microfibril is shown by connecting the circles belonging to the same microfibril. The crystals, which are needle-shaped at the beginning, may change to plates and connect in the later states of calcification (shaded area). A periodicity of 3.8 nm appears in the structure. **(b)** Quasi-hexagonal packing: Plate-shaped crystals (shaded area) are formed within adjacent holes (hexagones) and create a layered structure with a period of 3.8 nm as proposed in [23]. **(c)** Computer-generated, random distribution of HA-filled holes (hexagones) on a quasi-hexagonal lattice: Needles, plates, and even more complicated structures appear as crystal shapes. In contrast to the situations described in (a) and (b), this arrangement would not induce any superstructure peak in the SAXS spectrum which is in agreement with our data.

spectrum of embryonic bone whereas the lines corresponding to the crystal thickness, like the (310) line, should not be visible. This is in reasonable agreement with the work of Bonar et al. [21] where a crystal length of 10.7 nm was concluded from the breadth of the (002) line for embryonic chick bone, whereas the (310) line may hardly be seen in the diffraction pattern. Furthermore, we can not exclude by SAXS, even in embryonic bone, the existence of a small percentage of comparatively large crystals outside the collagen fibrils which could give rise to other diffraction lines in the wide-angle spectrum without affecting the small-angle scattering significantly. The second question concerns the magnitude of T ($\approx$3 nm) in adult bone. It seems hard to fit such large crystals into the collagen fibrils. As shown in Fig. 5, the collagen has to be compressed to provide the required space. This hypothesis is supported by recent neutron scattering results where the radial distance between collagen molecules was 1.53 nm in demineralized bone collagen and only 1.24 nm in bone [8]. Finally, it should be noted that due to the "Babinet principle," needle-shaped crystals surrounded by organic material cannot be distinguished by SAXS from long regions of organic matrix of the same thickness surrounded by mineral. The latter interpretation seems hypothetically attractive because it would suggest collagen molecules enclosed in a wall of mineral; it is, however, incompatible with the fact that the measured average thickness T increases with mineralization.

Concerning the possible equatorial arrangement (i.e., in the plane, perpendicular to the fibril axis) of mineral crystals within the gap zones of the fibrils, several models have been proposed in the past based on different hypotheses on the arrangement of the collagen molecules themselves. Based on the microfibrillar model [22], mineral deposition in tunnels between the microfibrils was proposed (Fig. 6a). Recently, a new model based on electron microscopic investigations was discussed [23], in which the arrangement of the organic molecules is supposed to be quasi-hexagonal [13] and the mineral crystals are thought to form a periodic succession of parallel plates (Fig. 6b). Both models propose a periodic arrangement of the mineral—needles in one case, plates in the other. This periodicity should induce an interference maximum in the radial scattering from bones. No such maximum was observed in any sample investigated in this study except the broad maximum at 1.3 nm, the basic repeat unit in the quasi-hexagonal array (Fig. 1).

The results of the present study could be explained by a model, as shown in Fig. 6c. In this assumption, mineral needles are distributed randomly, on a quasi-hexagonal lattice, as discussed also by others [24]. It is a characteristic of the random distribution (the configuration in Fig. 6c was generated by computer) that holes are sometimes located on neighboring sites. Consequently, not only isolated needles but also plate-like or even more complicated shapes could be found. It has to

be emphasized that the quasi-hexagonal arrangement of collagen molecules is a model for rat tail tendon which never mineralizes. In fact, the X-ray spectra of turkey tendon [25] and demineralized bone [26] only show broad diffuse peaks in the equatorial scattering, indicating a much less regular, probably short range, ordered structure. Correspondingly, the peak we found in the radial scattering from the mineral (Fig. 1) is also very week and broad (remember the logarithmic scales in Fig. 1). As a first approximation we have drawn a well-defined quasi-hexagonal lattice in Fig. 6c, but it would be easy to imagine that a distorted, only approximately hexagonal structure would provide even more randomness to the positions and shapes of the mineral crystals.

In conclusion, our data derived from SAXS suggest that mainly needle-like mineral crystals are located within the gap-zone of the collagen fibrils and arranged parallelly to the long axis of fibrils but without particular ordering in the equatorial plane. Adjacent needle-like crystals could then agglomerate to plate-like or even more complicated structures. During the maturation of long bones from the embryonal to the adult state, a progressive alignment of the crystals along the bone axis occurs. In contrast to long bones, calvariae did not show any anistropy in the orientation of the mineral needles. Finally, the thickness of the needles increased with bone maturation from 1.5 nm in embryonic to about 3 nm in adult mice and rats.

Acknowledgments: The authors thank Prof. Hanns Plenk for very enlightening discussions and comments. This work was supported in part by Lorenz-Böhler-Gesellschaft (Project No. 1/89) and Allgemeine Unfallversicherungsanstalt.

References

1. Posner AS (1987) Bone mineral and the mineralization process. In: Peck WA (ed) Bone and mineral research 5. Excerpta Medica, Amsterdam-Oxford-Princeton, pp 65–116
2. Glimcher MJ (1984) Recent studies of the mineral phase in bone and its possible linkage to organic matrix by protein-bound phosphate bonds. Trans R Soc Lond B304:479–508
3. Landis WJ, Paine MC, Glimcher MJ (1977) Electron microscopic observations of bone tissue prepared anhydrously in organic solvents. J Ultrastruct Res 59:1–30
4. Landis WJ, Hanuschka BT, Rogerson CA, Glimcher MJ (1977) Electron microscopic observations of bone tissue prepared by ultracryomicrotomy. J Ultrastruct Res 59:185–206
5. Lees S, Prostak K (1988) The locus of mineral crystals in bone. Conn Tissue Res 18:41–54
6. Ascenzi A, Bigi A, Koch MHJ, Ripamonti A, Roveri N (1985) A low-angle X-ray diffraction analysis of osteonic inorganic phase using synchrotron radiation. Calcif Tissue Int 37:659–664
7. Arsenault AL, Grynpas MD (1988) Crystals in calcified epiphyseal cartilage and cortical bone in the rat. Calcif Tissue Int 43:219–225
8. Bonar L, Lees S, Mook H (1985) Neutron diffraction studies of collagen in fully mineralized bone. J Mol Biol 181:265–270
9. Glatter O, Kratky O (eds) (1982) Small angle X-ray scattering. Academic Press, New York
10. Fratzl P, Fratzl-Zelman N, Klaushofer K, Hoffman O, Vogl G, Koller K (1989) Age-related changes of crystal size and orientation in bone tissue: a small-angle X-ray scattering study. Calcif Tissue Int (Suppl) 44:S91
11. Holmes JM, Beebe RA, Posner AS, Harper RA (1970) Surface areas of synthetic calcium phosphates and bone mineral. Proc Soc Exp Biol Med 133:1250–1253
12. Hodge AJ, Petruska JA (1963) Recent studies with the electron microscope on ordered aggregates of the tropocollagen molecule. In: Ramachandran GN (ed) Aspects of protein structure. Academic Press, London, pp 289–300
13. Hulmes DJS, Miller A (1979) Quasi-hexagonal molecular packing in collagen fibrils. Nature 282:878–880
14. Miller A, Wray JS (1971) Molecular packing in collagen. Nature 230:437–439
15. Guinier A, Fournet G (1955) Small angle scattering of X-rays. John Wiley, New York
16. Matsushima N, Akiyama M, Terayama Y (1982) Quantitative analysis of the orientation of mineral in bone from small angle x-ray scattering patterns. Jpn J Appl Phys 21:186–189
17. Sasaki N, Matsushima N, Ikawa T, Yamamura M, Fukuda A (1989) Orientation of bone mineral and its role in the anisotropic mechanical properties of bone-transverse anisotropy. J Biomechanics 22:157–164
18. Lees S (1987) Considerations regarding the structure of the mammalian mineralized osteoid from the viewpoint of the generalized packing model. Conn Tissue Res 16:281–303
19. White SW, Hulmes DJS, Miller A, Timmins PA (1977) Collagen mineral axial relationship in calcifed turkey leg tendon by X-ray and neuton diffraction. Nature 266:421–425
20. Kay MI, Young RA, Posner AS (1964) Crystal structure of hydroxyapatite. Nature 204:1050–1052
21. Bonar LC, Roufosse AH, Sabine WK, Grynpas MD, Glimcher MJ (1983) X-Ray diffraction studies of the crystallinity of bone mineral in newly synthesized and density fractionated bone. Calcif Tissue Int 35:202–209
22. Höhling H, Ashton BA, Fietzek PP (1980) Kollagenmineralisation. In: Kuhlencordt F, Bartelheimer H (eds) Klinische Osteologie A. Springer Verlag, Berlin, pp 59–80
23. Traub W, Arad T, Weiner S (1989) Crystal organization in Bone. Calcif Tissue Int (Suppl) 44:S94
24. Woodhead-Galloway J, Hugh Young W (1978) Probabilistic aspects of the structure of the collagen fibril. Acta Cryst A34:12–18
25. Brodsky B, Eikenberry EF, Belbruno KC, Sterling K (1982) Variation of collagen fibril structure in tendons. Biopolymers 21:935–951
26. Broek DL, Eikenberry EF, Fietzek PP, Brodsky B (1981) Collagen structure in tendon and bone. In: Veis A, (ed) The chemistry and biology of mineralized connective tissues. Elsevier, North Holland, pp 79–84

Received June 21, 1989, and in revised form October 3, 1989